scientific reports

Check for updates

OPEN

Exponential increase of transition rates in metastable systems driven by non-Gaussian noise

Adrian Baule[1]✉ & Peter Sollich[2,3]

Noise-induced escape from metastable states governs a plethora of transition phenomena in physics, chemistry, and biology. While the escape problem in the presence of thermal Gaussian noise has been well understood since the seminal works of Arrhenius and Kramers, many systems, in particular living ones, are effectively driven by non-Gaussian noise for which the conventional theory does not apply. Here we present a theoretical framework based on path integrals that allows the calculation of both escape rates and optimal escape paths for a generic class of non-Gaussian noises. We find that non-Gaussian noise always leads to more efficient escape and can enhance escape rates by many orders of magnitude compared with thermal noise, highlighting that away from equilibrium escape rates cannot be reliably modelled based on the traditional Arrhenius–Kramers result. Our analysis also identifies a new universality class of non-Gaussian noises, for which escape paths are dominated by large jumps.

Activated transitions between metastable states govern a large variety of phenomena in the physical, chemical, and biological sciences, ranging from chemical reactions to nucleation, self-assembly, and protein folding[1–4]. Following seminal works by Arrhenius, Eyring and Kramers, the description of transition rates has been well understood for systems at thermal equilibrium, for which the noise driving the transition is Gaussian: transition rates can be expressed in the generic form

$$r \simeq C\, e^{-\Delta V/T}, \tag{1}$$

where ΔV is the energy barrier that has to be crossed, in line with the Arrhenius factor $e^{-\Delta V/T}$ first derived in the context of reaction rate theory[5–7]. The prefactor C depends on the dimensionality of the problem and is determined by the curvatures at the bottom and top of the potential wells[1,6,7]. There is a remarkable variety of activated processes in equilibrium that have been shown to follow the Kramers result, with only the detailed form of C being model dependent[8]. However, many systems in the real world are intrinsically out-of-equilibrium due to active processes that drive their mechanical and dynamical properties, e.g., in biology[9]. As a result, the effective fluctuations can be non-Gaussian, such that escape events are not governed by Kramers' result.

In this work, we show that Eq. (1) is in fact a special case of a much more general expression that governs the escape behaviour in generic out-of-equilibrium systems driven by memoryless non-Gaussian fluctuations. Such fluctuations are ubiquitous in nature and have been shown to arise, e.g., in the dynamics of the cytoskeleton[10], intracellular transport[11–13], and small tracer particles interacting with swimming microorganisms[14–17]. They also occur in technologically relevant nanoscale systems such as strongly coupled qubits[18] and Josephson junctions[19–22], and are often used in phenomenological descriptions of macroscopic dynamics, e.g., for animal foraging[23,24], earthquake tremors[25], and financial markets[26]. Memoryless non-Gaussian fluctuations are also implicit in many models of active matter, such as the widely studied run-and-tumble particles and other models, that exhibit, e.g., motility induced phase transitions[28,29]. As we discuss below, these systems can also be treated within our approach.

We present a unified framework for such noise processes based on path-integrals where exact results for both the escape rate and the optimal escape path are obtained. In this approach the general form of the Kramers rate is recovered but with ΔV replaced by an effective action that depends on both the detailed functional form of the potential and the noise parameters. We show that the effective action is, in fact, always lower than ΔV for symmetric noise, highlighting that non-Gaussian noise generically leads to exponential speed-ups of transition rates. This speed-up can be dramatic, as we show for a realistic swimmer model, where transition rates are increased by 25 orders of magnitude compared with the Gaussian case. We also discover that escape processes driven by

[1]School of Mathematical Sciences, Queen Mary University of London, London E1 4NS, UK. [2]Institute for Theoretical Physics, Georg-August-University Göttingen, 37077 Göttingen, Germany. [3]Department of Mathematics, King's College London, London WC2R 2LS, UK. ✉email: a.baule@qmul.ac.uk

non-Gaussian noise can exhibit large jumps in the most likely transition path, forming a separate universality class among such processes that is distinguished further by a non-Kramers form of the transition rate prefactor C, which we calculate explicitly. All our results are confirmed by numerical simulations.

Results

We consider the time evolution of a single degree of freedom q, e.g. the position of a particle in one dimension, under the influence of a conservative force with potential V as well as noise ξ,

$$\dot{q}(t) = -V'(q) + \xi(t) \tag{2}$$

In Eq. (2), we assume that all quantities are dimensionless, see "Methods A: Dimensionless equation of motion". Metastability occurs when $V(q)$ exhibits two or more sufficiently deep potential wells such that the particle is mostly confined to the bottom of one of the wells, with rare escape events to neighbouring wells induced by the noise[1]. We study the *rates* for such escape events, in a framework that can be extended to systems with many degrees of freedom and non-conservative forces (which, for the Gaussian case, have been studied in[30]). Key to our setup is that $\xi(t)$ contains not only the conventional (Langevin) Gaussian white noise, but an additional non-Gaussian contribution that breaks detailed balance:

$$\xi(t) = \xi_{\mathrm{G}}(t) + \xi_{\mathrm{NG}}(t). \tag{3}$$

We take the latter as essentially the most general memoryless form of noise. This is Poissonian shot noise, which consists of a series of discrete 'kicks' arriving at rate λ_0:

$$\xi_{\mathrm{NG}}(t) = \sum_{j=1}^{N_t} A_j \delta(t - t_j) - \lambda_0 t \langle A \rangle . \tag{4}$$

Here the times t_j come from a Poisson process with rate λ_0, so that the total number N_t of kicks within a time interval $[0, t]$ follows a Poisson distribution with mean $\lambda_0 t$. Each kick size (amplitude) A_j is drawn independently from a fixed distribution with mean value $\langle A \rangle$. In Eq. (4), we subtract the resulting mean value of the shot noise such that $\langle \xi_{\mathrm{NG}}(t) \rangle = 0$ for any distribution of kick sizes.

While models of the form Eqs. (2)–(4) have been used on phenomenological grounds to model a large variety of processes in the sciences, recent work has also shown that the memoryless (or white) non-Gaussian noise of Eq. (4) arises as the result of systematic coarse-graining procedures in interacting particle systems. For example, in athermal granular systems coupled with a thermal reservoir, a system-size expansion shows that to leading order correlations with the environment can be neglected and white non-Gaussian fluctuations persist in addition to thermal Gaussian white noise[31,32]. Moreover, the dynamics of a passive tracer interacting with active particles in suspension can be shown to universally reduce to a process with Poisson statistics at low densities[33]. Memoryless non-Gaussian fluctuations then arise in the long-time regime and are manifest, e.g., in the non-Gaussian features of the tracer's displacement distribution[17], see also section "Comparison with simulations" below.

In order to investigate the dynamics of Eq. (2), we exploit the fact that the noise properties are captured by the cumulant generator (see "Methods B: Large deviation form of the path probability for non-Gaussian noise")

$$\ln \left\langle e^{i \int_0^t \mathrm{d}s\, \xi(s) g(s)} \right\rangle = \int_0^t \mathrm{d}s \left[\frac{D_0}{2} (ig)^2 + \lambda_0 \phi(iga_0) \right], \tag{5}$$

where ϕ is a moment generator defined as

$$\phi(u) = \int \mathrm{d}x\, \rho(x) \left(e^{ux} - ux - 1 \right) \tag{6}$$

The term $\frac{D_0}{2}(ig)^2$ in Eq. (5) represents the Gaussian white noise contribution, of variance D_0, while the second term $\lambda_0 \phi(iga_0)$ comes from the non-Gaussian kicks. We write the distribution of their amplitudes A as $\rho(A/a_0)/a_0$, where the parameter a_0 sets the characteristic amplitude scale and $\rho(x)$ is a baseline distribution. The amplitude scale of the distribution $\rho(x)$ can then be fixed, which we do by imposing $\int \mathrm{d}x\, x^2 \rho(x) = 1$. All noise statistics can be obtained from Eq. (5), e.g. $\langle \xi(t)\xi(t') \rangle = (D_0 + \lambda_0 a_0^2)\delta(t - t')$. Eq. (5) is in fact the most general form of the cumulant generator for a (zero mean) noise process ξ that is stationary and uncorrelated in time. This is also known as Lévy noise, and defined technically as the derivative of a process with independent stationary increments[26]. Our only restriction on this is the finiteness of $\int \mathrm{d}x\, x^2 \rho(x)$, to allow us to assign a scale to the noise variance. In this form the setting also covers cases where ρ is not normalizable, e.g. when it has a power law divergence $\rho(x) \propto |x|^{-\alpha-1}$ for small x[34] with $0 < \alpha < 2$. We focus in the following on symmetric noise with $\rho(x) = \rho(-x)$. Our analysis will show that escape properties depend crucially on the form of ρ; in fact we will be able to classify amplitude distributions ρ into three different types A, B and C as illustrated in Fig. 1. Broadly speaking, type A encompasses all noise distributions $\rho(x)$ with tails that—like e.g. Gaussians—decay faster than any linear exponential. Noise distributions of types B and C both have tails that are to leading order exponential, causing singularities in the moment generator $\phi(k)$ at finite k. The further distinction between them relies on whether, once the leading exponential decay factor has been removed, the distributions have integrals that diverge or converge for $x \to \infty$.

Equations (2)–(6) unify the description of non-Gaussian noise-induced activation studied previously, both analytically and numerically, for a range of special cases such as kicks with exponentially distributed[35–41] or constant amplitudes[42–44], and Lévy flights[45–52]. We also include in our considerations the form of ϕ obtained by

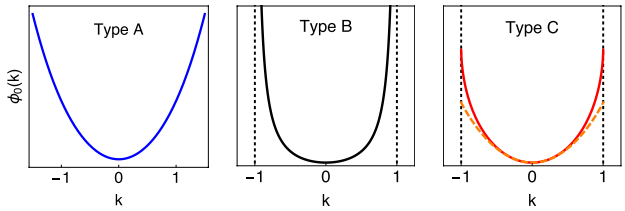

Distribution	Type	$\rho(x)$	$\phi(u) = \langle e^{ux} - ux - 1 \rangle$
Constant	A	$\frac{\delta(x-1)}{2} + \frac{\delta(x+1)}{2}$	$\cosh(u) - 1$
Exponential	B	$e^{-\lvert x\rvert}/4$	$u^2/[2(1-u^2)]$
Gamma α	C	$\frac{\lvert x\rvert^{-\alpha-1} e^{-\lvert x\rvert}}{2\Gamma(2-\alpha)}$	$\frac{(1+u)^\alpha + (1-u)^\alpha - 2}{2\alpha(\alpha-1)}$
Truncated ϕ	A		$\frac{1}{2}u^2 + bu^4$

Figure 1. We classify amplitude distributions ρ into three types according to their moment generator ϕ. Type A: ϕ is unbounded without singularities. Type B: ϕ diverges upon approaching two singularities, taken as lying at ± 1. Type C: ϕ is bounded with singularities at ± 1 in higher derivatives. Examples for each type are given, normalized as $\int \mathrm{d}x\, x^2 \rho(x) = 1$. For the Gamma distribution we assume $0 < \alpha < 2$ and show the cases $\alpha = 0.6$ (solid line) and $\alpha = 1.6$ (dashed).

expanding to the first non-Gaussian order (cubic in general, quartic in our symmetric case). This widely used approximation scheme corresponds to artificially setting to zero all higher cumulants of the noise amplitude distribution[19–22,44,53] and we will see that it can lead to qualitatively incorrect predictions. Our framework will also allow us to recover rigorous mathematical results on the dominant scaling of the escape rate for non-Gaussian noise for a specific weak-noise regime[54,55].

Path-integral framework. Our analysis of non-Gaussian escape rates is based on a path integral framework. As in the seminal Kramers escape rate calculation for Gaussian noise, we will consider a weak-noise regime. Fluctuations around the most likely escape path from one metastable state to another are then small and the typical path can be obtained by minimizing a stochastic action $S[q]$ w.r.t. to paths $q(s)$. The key technical steps in extending this approach to the non-Gaussian case with cumulant generator given by Eq. (5) are (see "Methods B: Large deviation form of the path probability for non-Gaussian noise"): (1) Following the Martin–Siggia–Rose formalism, the transition probability of the escape process is expressed as an integral over paths $q(s), g(s)$, where g is an auxiliary field conjugate to the noise. (2) We rescale the noise parameters by a dimensionless scaling parameter ϵ as

$$D_0 = D\,\epsilon, \qquad \lambda_0 = \lambda/\epsilon, \qquad a_0 = a\,\epsilon \tag{7}$$

The variance of the noise ξ is then $D_0 + \lambda_0 a_0^2 = (D + \lambda a^2)\epsilon \propto \epsilon$ so that the weak noise limit is $\epsilon \to 0$. While Eq. (7) may appear somewhat specific, it represents in fact a generic weak-noise regime that preserves all details of the non-Gaussian noise distribution ρ for small ϵ, not just the leading non-Gaussian cumulants as considered in[19–22,44] (see the discussion in "Rescaling the noise parameters"). We also emphasize that our final results can be converted back into expressions in terms of the original noise parameters D_0, λ_0, a_0 or into another weak-noise regime, see section "Special cases", highlighting the generality of our approach.

(3) The auxiliary field g can be integrated out by a saddle-point method for $\epsilon \to 0$. The net result for the path probability takes the large-deviation form

$$P[q] \propto e^{-\int_0^t \mathrm{d}s\, \mathcal{L}(\dot{q} + V'(q))/\epsilon}, \tag{8}$$

with the Onsager–Machlup-like Lagrangian $\mathcal{L}$ written only in terms of the physical paths $q(s)$. We find that $\mathcal{L}(\cdot)$ is given by the Legendre transform $\mathcal{L}(f) = \max_k[kf - \psi(k)]$ of

$$\psi(k) = Dk^2/2 + \lambda\phi(ak). \tag{9}$$

One can check that this result remains valid even when ϕ has singularities on the real axis; the maximum then has to be taken over the non-singular range. In the example cases shown in Fig. 1 such singularities occur for the exponential and Gamma noise amplitude distributions, which are of type B and C, respectively. In contrast, distributions with tails decaying faster than exponentially (type A) do not produce singularities in ϕ; see the constant modulus example in Fig. 1. We note for later that ϕ is convex and therefore so are ψ and the Lagrangian $\mathcal{L}$ as its Legendre transform. For our symmetric noise distributions, all three functions are also symmetric and thus have their global minimum at vanishing argument. The symmetry further ensures that all odd moments of x vanish while the even ones are positive, which from Eq. (6) implies the lower bound $\phi(u) \geq u^2/2$ and hence a similar bound $\psi(k) \geq (D + \lambda a^2)k^2/2$.

Effective action. Let us now consider escape from a metastable state q_a, located at the minimum of the metastable basin of V, across the top of the nearest potential barrier at $q_b > q_a$. For Gaussian noise, the path

integral solution of this problem[58–60] is analogous to the quantum mechanical tunneling problem treated in a semiclassical approximation[61] and gives the dominant scaling of the escape rate r for small ϵ as $r \cong C\, e^{-S_{\min}/\epsilon}$. In our general non-Gaussian case the equivalent form can be deduced from the theory of large deviations[62] for $\epsilon \to 0$ with the effective energy barrier given by the minimum action

$$S_{\min} = \lim_{t\to\infty} \min_{[q]} \int_0^t \mathrm{d}s\, \mathcal{L}(\dot{q} + V'(q)). \tag{10}$$

The minimum is over all paths with $q(0) = q_a$, $q(t) = q_b$, and the resulting optimal path (also called 'instanton' or 'excitation path') gives the typical escape trajectory for small ϵ. To make progress in determining $S_{\min}$, one can think of any $q(s)$ as a path in the (q, v)-plane, with $v = \dot{q}$. Then the action reads $\int \mathrm{d}q\, \mathcal{L}(v + V'(q))/|v|$ and for each q we can find $v = \dot{q}$ simply as the minimum of $\mathcal{L}(v + V'(q))/|v|$. We do not need to enforce the total time constraint $t = \int \mathrm{d}q/|v|$ as the minimal action path is obtained for $t \to \infty$, which is automatically fulfilled since the integral for t diverges at both ends for paths between stationary points of V. The trivial global minimum is $v = -V'(q)$, which describes deterministic relaxation. For an excitation from q_a to $q_b > q_a$, on the other hand, we have $V' > 0$ and need $v > 0$. If – and this is an important restriction as we will show—the minimum of $\mathcal{L}(v + V'(q))/v$ occurs at finite v, it obeys $\mathcal{L}(v + V'(q)) = v\mathcal{L}'(v + V'(q))$. This condition, together with the fact that $\mathcal{L}$ is the Legendre transform of ψ, i.e., $\mathcal{L}'(f) = k^*$ with $k^* = \mathrm{argmax}_k[kf - \psi(k)]$ yields for the minimum action the simple result

$$S_{\min} = \int_{q_a}^{q_b} \mathrm{d}q\, k^*(V'(q)), \tag{11}$$

where $k^*(V')$ is determined from

$$V'(q) = \psi(k^*)/k^*. \tag{12}$$

This expression is just our minimum condition $\mathcal{L}(f) = vk^*$ rewritten using $\mathcal{L}(f) = k^*f - \psi(k^*)$ and $f = v + V'$. The inverse Legendre transform relation $\psi'(k^*) = f$ yields further

$$v = \dot{q} = \psi'(k^*) - V'(q). \tag{13}$$

Together with Eq. (12) this defines a velocity function $\dot{q} = \Xi(V'(q))$ that characterizes the shape of the instanton.

By comparing Eq. (11) with the classical mechanics result $\partial S/\partial q = p$ one sees that our k^* plays exactly the role of momentum, while the minimization condition $k^*V'(q) = \psi(k^*)$ corresponds to the well-known condition that the Hamiltonian $\mathcal{H} = k^*\dot{q} - \mathcal{L} = -k^*V'(q) + \psi(k^*)$ must vanish on minimum action paths of duration $t \to \infty$[41,42]. However, we will discover below that minimal action paths can in certain cases contain jumps, in which case the criterion $\mathcal{H} = 0$ ceases to be applicable because $\dot{q}$ becomes undefined. Our approach of minimizing $\mathcal{L}(v + V'(q))/|v|$ will continue to be valid, on the other hand.

Gaussian vs non-Gaussian escape. Analysing the effective energy barrier $S_{\min}$ for arbitrary non-Gaussian noise types yields striking differences with the Gaussian case summarized as follows: (i) On replacing a Gaussian noise by a non-Gaussian one of the same variance, the escape rate always increases, i.e. non-Gaussian noise is at least as efficient as Gaussian noise: $S_{\min} < 2\,\Delta V/(D + \lambda a^2) \equiv S_{\mathrm{G}}$ for any distribution of type A, B or C, see Fig. 2a,b. The reference value S_{G} here is the activation barrier that results when the non-Gaussian noise is replaced by Gaussian noise of the same variance, corresponding to the truncation of the Taylor expansion of $\phi(k)$ after the quadratic term. Because $S_{\min}$ enters the escape rate as $\exp(-S_{\min}/\epsilon)$, non-Gaussian noise thus offers *exponential* speed-ups. (ii) Remarkably, for amplitude distributions of types B and C even noise of infinitesimal intensity $\lambda \to 0$ yields a value of $S_{\min}$ considerably smaller than S_{G}, indicating a singular limit. (iii) Optimal escape paths have the characteristic instanton shape, with the particle moving rapidly from the initial minimum to the transition state at the top of the barrier, but the shape varies with ϕ. This contrasts with the Gaussian noise case, where excitation paths are, in the situation we consider, simply the time-reverse of deterministic relaxation paths (Fig. 2). In $d = 1$ it is sufficient for the noise to be additive, as we assume, for this statement to hold. In higher dimensions it holds e.g. when the noise is additive and isotropic and the force is derived from a potential. (iv) For type C amplitude distributions we identify an entire region in the (a, λ) parameter plane where the escape paths contain a *discontinuous jump* (Fig. 2). Note that the behaviours (ii) and (iv) cannot be reproduced with any cumulant truncation, as this effectively produces a type A form of $\phi(k)$.

We proceed to explain all of these observations on the basis of the properties of the noise amplitude moment generator ϕ. Firstly we saw above that $\psi(k) \geq (D + \lambda a^2)k^2/2$, which implies from Eq. (12) that $k^* \leq 2V'/(D + \lambda a^2)$. With Eq. (11) the reduction (i) of the effective barrier, $S_{\min} < S_{\mathrm{G}}$, follows directly.

To analyse the limit of small λ we consider the solutions of Eq. (12), which using Eq. (9) can be cast in the form

$$V'(q) = \frac{D}{2}\, k^* + \lambda \frac{\phi(ak^*)}{k^*}. \tag{14}$$

Rewriting further one can show that in order to see strongly non-Gaussian behaviour the noise amplitude has to lie in the range $1 \ll a \ll 1/\lambda$ (see "Methods C: Analysis of the escape behaviour"), which in turn requires $\lambda \ll 1$. Considering accordingly $\lambda \to 0$ for fixed a, the last term in Eq. (14) disappears, suggesting that $k^* = 2V'/D$, which yields Gaussian behaviour. This argument always works for amplitudes of type A, while for type B it only holds if $k^* = 2V'/D$ remains smaller than the singularity in $\phi(ak)$ at $1/a$, i.e., when

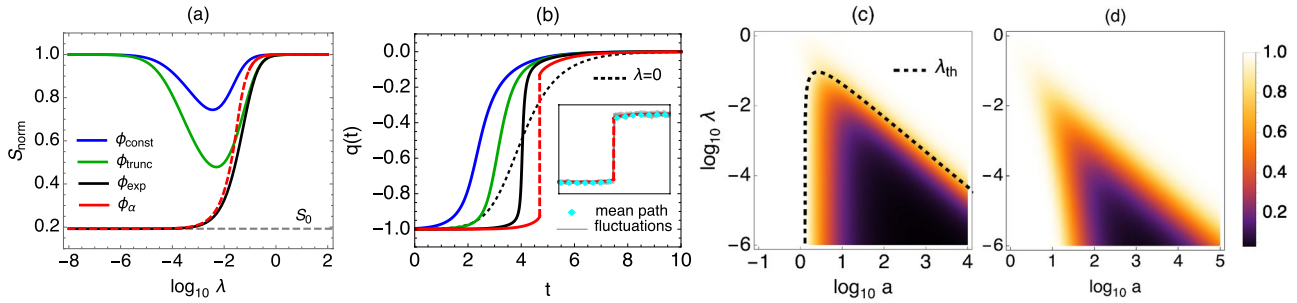

Figure 2. (**a**) The normalized action $S_{\rm norm} = S_{\rm min}/S_{\rm G}$ for the different ϕ of Fig. 1 ($a = 10, \alpha = 0.8, b = 1/2$, $D = 1$) and the potential $V(q) = q^4/4 - q^2/2$. Noise amplitude distributions of type A ($\phi_{\rm const}, \phi_{\rm trunc}$) recover the Gaussian value $S_{\rm norm} = 1$ as $\lambda \to 0$. For type B and C amplitudes ($\phi_{\rm exp}, \phi_\alpha$), $S_{\rm norm}$ decreases monotonically as $\lambda \to 0$ and converges to a nontrivial limit S_0, Eq. (15). The action for ϕ_α corresponds to an escape path with a discontinuous jump when $\lambda < \lambda_{\rm th}$ (red dashed line). (**b**) Instanton escape paths for the different ϕ showing a rapid motion from the initial minimum to the barrier; for ϕ_α the instanton has a jump section. Colors, potential, and parameters as in (**a**) (apart from $\alpha = 1.2$ and $\lambda = 0.01$). For non-Gaussian noise the time-reversal symmetry between excitation and relaxation paths is broken, seen here by the difference with the slower $\lambda = 0$ instanton of the Gaussian dynamics (dotted line). Inset: Mean path sampled numerically from the path weight for $\epsilon = 0.01$ compared with theory for ϕ_α, confirming the jump. (**c**, **d**) Colour maps of $S_{\rm norm}$ for (**c**) ϕ_α with $\alpha = 0.8$ and (**d**) $\phi_{\rm const}$. The dashed line is the phase boundary $\lambda_{\rm th}(a)$ separating regions with smooth ($\lambda \geq \lambda_{\rm th}$) and jump ($\lambda < \lambda_{\rm th}$) instantons.

$2V'/D < 1/a$. If instead $2V'/D > 1/a$, the solution of Eq. (14) approaches $k^* = 1/a$ for $\lambda \to 0$, since $\phi(ak)$ diverges for $k \to 1/a$ and the last term in Eq. (14) eventually becomes dominant. Overall, one therefore obtains $k^*(V') \to \min(2V'/D, 1/a)$ and the effective energy barrier $S_{\rm min} \to S_0$ where from Eq. (11)

$$S_0 = \int_{q_a}^{q_b} {\rm d}q \, \min(2V'(q)/D, 1/a) \tag{15}$$

The value S_0 that is approached as $\lambda \to 0$ lies *below* $S_{\rm G}$ for $1/a < 2\max_q V'(q)/D$, making the limit discontinuous (see Fig. 2). The discontinuity is possible as we have implicitly taken the limit $\epsilon \to 0$, where the unscaled rate λ_0 is large for any $\lambda > 0$ from Eq. (7). Since for type B noise $\phi'(ak)$ and thus $\psi'(k)$ diverge for $k \to 1/a$, Eq. (13) tells us that the velocity v becomes very large on the sections of the instanton with $1/a < 2V'/D$, so that the path in that region becomes closer and closer to a discontinuous jump as λ decreases. On the other hand, on the sections with $1/a > 2V'/D$, Eq. (13) yields the Gaussian shape.

Remarkably, for type C, the boundedness of ϕ implies that Eq. (14) will not have a solution when V' lies above a threshold $V'_{\rm th} = \max_k \psi(k)/k = D/(2a) + \lambda a \phi(1)$. This condition is met on at least part of the instanton when $\lambda < \lambda_{\rm th} = [\max_q V'(q) - D/(2a)]/[a\phi(1)]$. In the range of q where $V'(q) > V'_{\rm th}$ our approach shows its key benefit over the standard Euler-Lagrange equations or the criterion $\mathcal{H} = 0$, neither of which have solutions in this regime because $\dot{q}$ becomes undefined: one can check here that $\mathcal{L}(v + V'(q))/v$ is monotonically decreasing for $v > 0$, reaching the limit $1/a$ for $v \to \infty$: the optimal velocity is infinite, $\Xi(V'(q)) = \infty$. This implies that there must be a jump in the optimal path whenever $\lambda < \lambda_{\rm th}$. To the action this jump contributes $\int {\rm d}q/a = \Delta q/a$ where the integral covers the relevant q-range and gives the length Δq of the jump. The contribution of the rest of the path has to be found by solving Eqs. (12) and (13) as before, which produces the Gaussian shape for $\lambda \ll 1$. The condition $\lambda < \lambda_{\rm th}$ maps out a dynamical phase diagram in the (a, λ) plane separating jump and no-jump escape behaviours (see Fig. 2c).

Since the threshold $V'_{\rm th} \to D/(2a)$ for $\lambda \ll 1$, the escape behaviour for noise amplitude distributions of type B and C becomes identical in this regime: the instanton consist of initial and final segments of time-reversed relaxations, connected by a jump, and the resulting action is S_0, Eq. (15). We remark that the class of amplitude distributions with this property can be characterized generally as distributions with exponentially decaying tails, i.e. of the form $\rho(x) = c(x)e^{-|x|}$, with $\lim_{x\to\pm\infty} \ln(c(x))/x = 0$. These two conditions are sufficient for the existence of a singularity in $\phi(u)$ at $u = 1$, see Eq. (6). Jump instantons at finite λ as in type C appear when, in addition, the condition $\int_1^\infty {\rm d}x \, c(x) < \infty$ is satisfied, since then $\phi(1)$ is finite.

Special cases. Our general solution in Eqs. (11)–(13) reproduces existing results in the literature for specific amplitude distributions. As a sanity check, we find in the Gaussian case ($\lambda = 0$) $\psi(k) = Dk^2/2$; thus $k^* = 2V'/D$, which with Eq. (11) and the Einstein relation $D\epsilon = D_0 = 2T$ recovers the van't Hoff–Arrhenius scaling $\sim e^{-\Delta V/T}$ of the escape rate. The instanton obeys $\dot{q} = V'(q)$ from Eq. (13), which as expected for Gaussian noise is the time reverse of a noise-free deterministic relaxation path[58–60]. For escape driven by one-sided exponentially distributed amplitudes without a Gaussian component, we have $\phi(u) = u^2/(2(1-u))$ and solving Eq. (12) for k^* yields $k^* = 2V'/(\lambda a^2 + 2aV')$ as obtained in[35,36,39]. We likewise recover analytical results for the effective action derived for one-sided constant and two-sided exponentially distributed amplitudes[41,42], see "Methods C: Analysis of the escape behaviour".

Rigorous mathematical results for the escape rates of Eqs. (2)–(6) have been obtained in[54,55] for a different scaling regime of the noise parameters. Remarkably, our large deviation approach is able to recover these results for those amplitude distributions for which ϕ from Eq. (6) is well-defined. Instead of Eq. (7), the parameter scaling adopted in[54,55] is given by

$$D_0 = \epsilon^2, \qquad \lambda_0 = 1, \qquad a_0 = \epsilon, \tag{16}$$

which leads to a weak-noise regime with a constant rate of non-Gaussian noise kicks and intensity $D_0 + \lambda_0 a_0^2 = \epsilon^2$. We can retrieve this scaling by setting $D = \lambda = \epsilon'$ and $a = 1$ *after* the rescaling in Eq. (7) that leads to the large deviation form of the action. We then take ϵ' as small and identify $\epsilon' = \epsilon$ at the end. Now for $\epsilon' \ll 1$ the solutions of Eq. (14) satisfy

$$V'(q) = \frac{\epsilon'}{2}k^* + \epsilon' \frac{\phi(k^*)}{k^*} \approx \epsilon' \frac{\phi(k^*)}{k^*}, \tag{17}$$

since k^* will become large for small ϵ' and $\phi(u)$ increases at least exponentially for large k^*. Two classes of amplitude distributions discussed in[54,55] are bounded amplitudes such as the constant amplitudes of Fig. 1, and amplitude distributions with super-exponentially decaying tails, $\rho(x) \propto \exp(-x^\gamma)$ with $\gamma > 1$. For the former we have $\phi(u) \sim e^{bu}$ for $u \gg 1$, where b is the upper bound, and for the latter $\phi(u) \sim \exp\left[(\gamma-1)(u/\gamma)^{\gamma/(\gamma-1)}\right]$. Determining then the asymptotic solutions of Eq. (17) for $\epsilon' \ll 1$ and substituting into Eq. (11) with $\epsilon' = \epsilon$ yields the dominant terms in the effective action for $\epsilon \to 0$ as

$$S_{\min} \approx (q_b - q_a)|\ln \epsilon| \tag{18}$$

for bounded amplitudes and

$$S_{\min} \approx (q_b - q_a)\gamma(\gamma-1)^{(1-\gamma)/\gamma}|\ln \epsilon|^{(\gamma-1)/\gamma} \tag{19}$$

for amplitude distributions with super-exponentially decaying tails. Eqs. (18,19) are precisely the results obtained in[54,55] for $r \propto e^{-S_{\min}/\epsilon}$ and $\epsilon \ll 1$. We note that our approach is not able to reproduce the corresponding expressions for amplitude distributions that decay with power-law or sub-exponential tails calculated in[54,55] since in these cases $\phi(u)$ is undefined for any nonzero real u.

Prefactor. The effects discussed above relate to the exponential term in the rate of escape processes $r \simeq C\exp(-S_{\min}/\epsilon)$, with non-Gaussian noise producing exponential speed-ups by reducing $S_{\min}$. We have also studied the prefactor C, to see whether this modifies the results. Recent work has shown that C can be determined by solving matrix Riccati equations, which is particularly suitable for numerical evaluations[56,57]. Analytical expressions for C have previously been obtained e.g. by calculating the fluctuation determinant in the path integral approach[58,59,63] or by determining steady state solutions[1,7] of the Fokker–Planck equation associated with Eq. (2), augmented by an injection term near q_a. We have used both these methods to confirm that in the regime where the excitation path is smooth, the prefactor is exactly the *same* as in the Gaussian case, i.e. given by the Eyring-Kramers expression $C = \sqrt{V''(q_a)|V''(q_b)|}/(2\pi)$[64], as observed previously for special cases of our noise[35,41].

However, C is modified when the excitation path has a jump section. The path integral method breaks down here because the eigenfunction expansion of the relevant fluctuation operator becomes ill-defined. However, determining the flux over the barrier in steady state remains feasible. We report the technically non-trivial calculation elsewhere[64]. The result applies generally to noise distributions $\rho(x) = c(x)e^{-|x|}$ with exponential cutoff and power law tails, $c(x) \simeq c_\alpha x^{-\alpha-1}$ for $x \gg 1$. We find

$$C = c_\alpha \epsilon^\alpha \lambda[(q_+ - q_-)/a]^{-\alpha-1}\left(\frac{V''(q_a)|V''(q_b)|}{V''(q_-)|V''(q_+)|}\right)^{1/2} \tag{20}$$

if the jump is from q_- to q_+. The key observation here is that while the prefactor is no longer independent of ϵ, its power law variation ϵ^α is much weaker than the exponential $\exp(-S_{\min}/\epsilon)$. For small ϵ non-Gaussian noise therefore still generates vastly faster escapes from metastable states than Gaussian noise of the same variance. We also observe in Eq. (20) that the (scaled) rate λ of the non-Gaussian noise enters as a prefactor, demonstrating that the escape dynamics is largely controlled by non-Gaussian effects. These must then disappear for $\lambda = 0$ or more precisely, by comparing with the Kramers rate, when λ becomes of $\mathcal{O}(e^{-(S_G - S_0)/\epsilon})$.

The final factor in Eq. (20) contains the curvature information from the Kramers prefactor $(V''(q_a)|V''(q_b)|)^{1/2}$ but effectively corrects this by the relevant curvatures at the beginning and end of the jump, i.e. the term is divided by $(V''(q_-)|V''(q_+)|)^{1/2}$. Note that the remaining factors can be written as $\lambda\epsilon^{-1}c((q_+ - q_-)/(\epsilon a))$ using the large x-behaviour of $c(x)$, and in that form should be generic for other, less than exponentially varying, forms of $c(x)$ that produce discontinuous excitation paths. This contribution to C is essentially the probability of receiving a noise "kick" that will perform the required jump. The exponential factor $e^{-|x|} = e^{-(q_+ - q_-)/(\epsilon a)}$ from $\rho(x)$ that should also appear here is accounted for in the action $S_{\min}$ and is exactly the jump contribution to $S_{\min}$ we identified earlier.

Comparison with simulations. To check our theoretical predictions, we implemented different simulation algorithms to determine the escape rates numerically. The Langevin dynamics can be simulated with standard methods based on an Euler discretization of Eq. (2)[26], but escape events become exceedingly rare as $\epsilon \to 0$

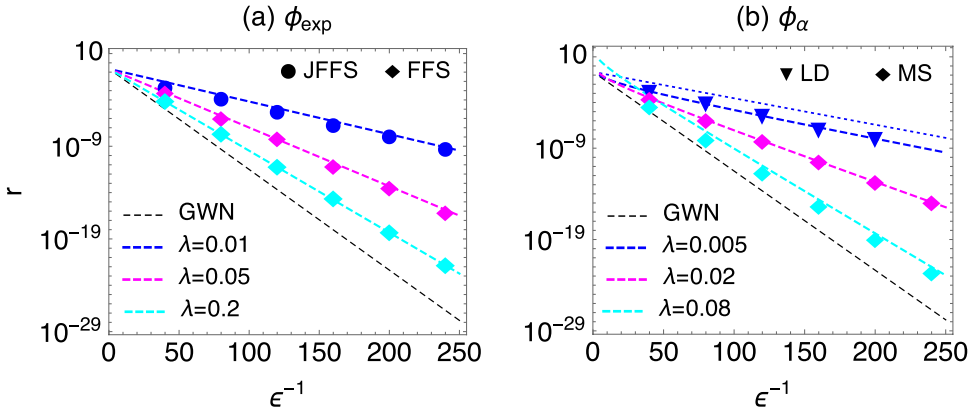

Figure 3. Comparison of the theoretical predictions (lines) for the escape rate r and results from numerical simulations. We have employed forward-flux sampling (FFS), jumpy forward-flux sampling (JFFS), direct Langevin simulations (LD), and a numerical solution of the Master equation (MS). The potential is $V(q) = q^4/4 - q^2/2$, $D = 1$, and we have set the rescaled noise intensity λa^2 of the non-Gaussian component also to unity, i.e., $a = 1/\sqrt{\lambda}$, which leaves λ as the only free parameter. Dashed black line: escape rates for purely Gaussian noise of the same noise intensity (GWN), highlighting exponential speed-ups due to non-Gaussian effects. (**a**) PSN with exponentially distributed amplitudes, leading to smooth instantons. (**b**) Gamma noise with $\alpha = 0.8$, leading to jump instantons for $\lambda = 0.005$ and $\lambda = 0.02$; the predicted jump prefactor (20) clearly gives a better description of the data than the Eyring-Kramers prefactor (dotted line for $\lambda = 0.005$). In both (**a**) and (**b**) the largest escape rates are achieved for $\lambda \to 0$, see also Fig. 2a.

and measuring very small rates thus requires suitable rare-event sampling algorithms. In the parameter regime in which the instanton is smooth, we have used forward-flux sampling (FFS)[65] and jumpy FFS[66] to confirm the theoretical predictions, see Fig. 3a, reaching rates as small as $r \approx 10^{-22}$. These methods are not applicable when the instanton has jumps, since for escape events with jumps the partitioning of the coordinate space into neighbouring bins as used in FFS becomes meaningless. In the jump regime, we thus used direct Langevin simulations (DL) and, in order to reach smaller rates, a numerical solution of the Master equation associated with Eq. (2) (MS), which confirm our theory and demonstrate in particular the validity of the prefactor Eq. (20), see Fig. 3b.

Figure 3 highlights the exponential increase of escape rates due to non-Gaussian noise, which results in speed-ups of up to 20 orders of magnitude for the same noise intensity. Conversely, this dramatic difference implies that assessing the effect of fluctuations on transition rates from their variance alone is unreliable and can drastically underestimate the true transition rate. To elucidate this point further we investigated a realistic non-Gaussian noise-driven system to compare our predictions with the Kramers theory. We simulate non-interacting swimmers in a three dimensional volume interacting with a passive tracer particle via a truncated dipolar force that describes the hydrodynamic interaction in the far-flow field regime at low Reynolds numbers[17]. As shown in[17], the stochastic motion of the tracer is effectively driven by non-Gaussian noise described by Eqs. (2) and (6), provided the dynamics is observed on sufficiently long time scales. Trapping the tracer in the double well potential $V(q) = V_0\left[(q/q_0)^4/4 - (q/q_0)^2/2\right]$, we measure the escape rate as

$$r \approx 2 \cdot 10^{-6} \tag{21}$$

for $V_0 = 5 \cdot 10^{-6}$ and $q_0 = 25$. These parameters have been adjusted such that escape times are short enough to be measurable (while they would be astronomically long for Gaussian noise, see below), but also sufficiently long to probe the Markovian regime of the tracer dynamics; all remaining parameters are set as in[17]. Calculating the escape rate with Eqs. (9), (11) and (12) where ϕ is fitted from the empirical tracer displacement statistics (see "Methods D: Escape rate calculation for a tracer particle diffusing in an active suspension") yields a rate of $r \approx 6 \times 10^{-4}$. While this differs by two orders of magnitude from the measured rate in Eq. (21), Kramers rate theory based on the diffusion coefficient of the tracer would give $r \approx 5 \times 10^{-32}$(!), again emphasizing that ignoring the non-Gaussian characteristics of the tracer can lead to dramatically inaccurate predictions. The discrepancy of two order of magnitude in the escape rate can be attributed both to the fact that the noise underlying the tracer dynamics is only approximately a memoryless non-Gaussian noise as expressed in Eq. (6), and to pre-asymptotic effects arising from the fact that the exponent $S_{\min}/\epsilon$ we obtain in the calculation of the escape rate is of order unity.

Discussion

Our results demonstrate that non-Gaussian noise can induce qualitatively very different escape behaviours. The instantons with jump section, occurring within the jump phase shown in Fig. 2c, indicate an escape strategy that is fundamentally different from the one we find in thermal equilibrium systems: instead of completing the entire escape using a rare sequence of small fluctuations, the system prefers to wait for a single rare fluctuation that is large enough to carry it across the steepest section of the potential barrier. Remarkably, the prefactor C highlights the existence of two universality classes associated with these two types of escape: the Kramers

prefactor, which also applies to non-Gaussian noise in the parameter range where the escape path is smooth; and Eq. (20) governing the jump escape.

The theoretical analysis shows that the exponential speed-up of transition rates can persist and become even more pronounced in the regime $\lambda \to 0$ (for constant a), i.e. when the intensity of the non-Gaussian contribution in Eq. (3) is vanishingly small, see Fig. 2a. It might be possible to exploit this effect to optimize switching behaviour in artificial systems driven by non-Gaussian noise such as colloids interacting with an active microbial heat bath on which thermodynamic cycles can be imposed[15]. Indeed, recent experiments have shown that non-Gaussian noise can be used to tune the performance of a colloidal Stirling engine by shifting the operating speed at which power is maximum[67].

The generalisation of our model Eq. (2) to higher dimensions includes e.g. non-Gaussian noise effects from copy number fluctuations in chemical reactions, which for a specific case were studied in[68], and widely used active particle models such as run-and-tumble particles[27,28]. Taking the latter case in two dimensions, one would have position coordinates (q_x, q_y) and the orientation angle θ of the active force that receives non-Gaussian noise kicks during tumbling events. With our approach one could, in particular, study the regime where tumbling and diffusion are of comparable strength, rather than the simpler situation where tumbling is so fast that the active force direction becomes effectively slaved to the particle position[69]. Our method also allows a systematic investigation of non-Gaussian noise effects on activation processes observed in other models for active particle motion[70] and opens up many further fascinating questions, e.g., how non-Gaussian noise affects the selection of the transition states that are traversed during the escape from a metastable state.

Methods A: Dimensionless equation of motion. We consider the overdamped motion of the position coordinate q under the effect of the potential $V(q)$ in one dimension

$$\gamma\, \dot{q}(t) = -V'(q) + \xi(t), \tag{22}$$

where γ denotes the friction coefficient and ξ noise from the environment. We assume that $V(q)$ can be expressed as $V(q) = V_0 \tilde{V}(q/q_0)$, where V_0 and q_0 set the energy and spatial scales, respectively, and $\tilde{V}$ is dimensionless. The scale of time can then be set by $t_0 = q_0^2\gamma/V_0$. Introducing dimensionless time and position as $\tilde{q} = q/q_0$ and $\tilde{t} = t/t_0$ yields

$$\frac{\mathrm{d}\tilde{q}(\tilde{t})}{\mathrm{d}\tilde{t}} = -\tilde{V}'(\tilde{q}) + \frac{t_0}{\gamma q_0}\xi(t_0\tilde{t}). \tag{23}$$

Defining the dimensionless noise as

$$\tilde{\xi}(\tilde{t}) = \frac{t_0}{\gamma q_0}\xi(t_0\tilde{t}) \tag{24}$$

leads to Eq. (2) in the main text, with the tildes dropped from variable names for clarity.

It is straightforward to check that Eq. (24) correctly transforms the specific noise parameters into dimensionless quantities. Assuming first $\xi(t) = \xi_{\mathrm{G}}(t)$ as Gaussian white noise with noise intensity D_0, i.e. $\langle \xi(t)\xi(t')\rangle = D_0\gamma^2\delta(t-t')$, Eq. (22) with $V(q) = 0$ implies that $\langle q^2(t)\rangle = D_0\, t$ and thus D_0 has dimensions $[D_0] = [q_0]^2/[t_0]^2$ as expected for a diffusion coefficient. The dimensionless noise intensity is then $\tilde{D}_0 = D_0 t_0/q_0^2$ and the dimensionless noise has variance $\langle\tilde{\xi}(\tilde{t})\tilde{\xi}(\tilde{t}')\rangle = [t_0/(\gamma q_0)]^2 D_0\gamma^2\delta(t_0(\tilde{t}-\tilde{t}')) = (D_0 t_0/q_0^2)\delta(\tilde{t}-\tilde{t}') = \tilde{D}_0\delta(\tilde{t}-\tilde{t}')$. In the literature our D_0 is often written as $2D_0$ and $\tilde{D}_0$ as $2\tilde{D}_0$; we omit the factor of 2 in order to have $\tilde{D}_0$ directly related to the noise variance.

Secondly, let us assume that the noise $\xi(t) = \xi_{\mathrm{NG}}(t)$ is given by the Poissonian shot noise of Eq. (4). From the fact that ξ/γ has the same dimension as $\dot{q}$, one sees that $[A_j] = [\gamma][q_0]$. The dimensionless amplitudes are thus given by $\tilde{A}_j = A_j/(\gamma q_0)$ consistent with Eq. (22). In addition, the dimensionless rate is $\tilde{\lambda}_0 = \lambda_0 t_0$, which preserves $\tilde{\lambda}_0\tilde{t} = \lambda_0 t$; the average number of noise kicks is therefore unaffected by the change to dimensionless units as it must be.

Methods B: Large deviation form of the path probability for non-Gaussian noise. *The cumulant generator for non-Gaussian noise with independent stationary increments.* For the Poissonian shot noise of Eq. (4), we see that the increments $\bar{\xi}(s) \equiv \int_s^{s+\Delta t}\xi_{\mathrm{NG}}(s')\mathrm{d}s'$ over a small time step Δt are all independent and assume the values $\bar{\xi}(s) = A$ with probability $\lambda_0\Delta t$ and $\bar{\xi}(s) = 0$ otherwise. The characteristic function of a given increment is thus

$$\begin{aligned}\langle e^{ig(s)\bar{\xi}(s)}\rangle &= \langle e^{ig(s)A}\lambda_0\Delta t + 1(1-\lambda_0\Delta t)\rangle \\ &\approx \exp\left(\lambda_0\Delta t\langle e^{ig(s)A} - 1\rangle\right),\end{aligned} \tag{25}$$

with the remaining average taken over the amplitude distribution ρ_0. In general one wants the noise to have zero mean. Subtracting the constant average $\langle\xi(t)\rangle$ to enforce this in Eq. (4) gives an extra term $-ig(s)A$ inside the average of Eq. (25). Adding also in Eq. (4) a Gaussian noise contribution with variance D_0 we obtain

$$\langle e^{ig(s)\bar{\xi}(s)}\rangle = \exp\left(-\frac{D_0}{2}g(s)^2\Delta t + \lambda_0\phi_0(ig(s))\Delta t\right), \tag{26}$$

where ϕ_0 is given as

$$\phi_0(k) = \int \mathrm{d}A\, \rho_0(A)\left(e^{kA} - kA - 1\right). \tag{27}$$

As explained in the main text we find it useful to write $\rho_0(A) = \rho(A/a_0)/a_0$ in terms of a characteristic scale a_0 and a base distribution ρ, normalized so that $\int \mathrm{d}x\, x^2\rho(x) = 1$. For ϕ_0 this scaling implies $\phi_0(k) = \phi(ka_0)$, where

$$\phi(u) = \int \mathrm{d}A\, \rho(A)\left(e^{uA} - uA - 1\right). \tag{28}$$

and the normalization of ρ simplifies the non-Gaussian noise variance to $\lambda_0\langle A^2\rangle = \lambda_0 a_0^2$. Considering a whole noise trajectory and the continuum limit $\Delta t \to 0$ recovers the noise cumulant generator Eq. (5).

MSR action functional. In order to develop a path integral description of the dynamics Eq. (2) we again consider first a discretization into small time steps Δt. Using an Ito convention Eq. (2) can be discretized as

$$q(s + \Delta t) = q(s) + \Delta t\, V'(q(s)) + \bar{\xi}(s). \tag{29}$$

Enforcing the dynamics Eq. (29) at every time step with delta functions, we can express the probability of a path $[q] = (q(0), q(\Delta t), \ldots, q(t))$ with fixed $q(0)$ as a product

$$P[q] = \left\langle \prod_{s=0}^{t-\Delta t} \delta(q(s + \Delta t) - q(s) + \Delta t\, V'(q(s)) - \bar{\xi}(s)) \right\rangle. \tag{30}$$

The average is over the noises $\bar{\xi}(s) \equiv \int_s^{s+\Delta t} \xi(s')\mathrm{d}s'$ and can be done independently for each time step. Fourier transforming one such step gives

$$\int \frac{\mathrm{d}g(s)}{2\pi} e^{-ig(s)[q(s+\Delta t)-q(s)+\Delta t\, V'(q(s))]} \langle e^{ig(s)\bar{\xi}(s)}\rangle = \int \frac{\mathrm{d}g(s)}{2\pi} e^{-ig(s)[q(s+\Delta t)-q(s)+\Delta t\, V'(q(s))] - \frac{D_0}{2}g(s)^2\Delta t + \lambda_0\phi(ig(s)a_0)\Delta t} \tag{31}$$

using Eq. (26). Collecting the contributions from all time steps and taking $\Delta t \to 0$ gives the path probability in terms of a Martin–Siggia–Rose (MSR)-type action $S[q, g]$[71,72]:

$$P[q] = \int \mathcal{D}\left[\frac{g}{2\pi}\right] e^{-S[q,g]} \tag{32}$$

$$S[q, g] = \int_0^t \mathrm{d}s \left\{ ig(s)[\dot{q}(s) + V'(q(s))] + \frac{D_0}{2} g(s)^2 - \lambda_0\phi(ig(s)a_0) \right\} \tag{33}$$

Rescaling the noise parameters. The seminal Kramers escape rate for Gaussian noise ($\lambda = 0$) can formally be derived from the theory of large deviations that is applicable in the weak-noise limit $D_0 \to 0$. Fluctuations around the most likely path from one metastable state to another are then small and the typical path can be obtained by making the action $S[q]$ stationary w.r.t. $q(s)$ and $g(s)$. In order to analyse such a weak-noise regime, we introduce a dimensionless scaling parameter ϵ and rescale D_0 as

$$D_0 = D\,\epsilon, \tag{34}$$

such that the weak-noise regime is equivalent to taking $\epsilon \to 0$. Setting $\delta S/\delta g(s) = 0$ (still for $\lambda = 0$) gives $D\epsilon g = i(\dot{q} + V')$, showing that in the low-ϵ limit one needs to scale $g = \tilde{g}/\epsilon$. The action then becomes

$$S[q, \tilde{g}] = \frac{1}{\epsilon}\int_0^t \mathrm{d}s \left\{ i\tilde{g}[\dot{q} + V'(q)] + \frac{\tilde{g}^2}{2} - \lambda_0\epsilon\phi(i\tilde{g}a_0/\epsilon) \right\} \tag{35}$$

Without the non-Gaussian term this already has the desired scaling with ϵ^{-1} that shows how path fluctuations away from the most likely path become exponentially suppressed for small ϵ.

For nonzero λ the task now is to identify a scaling regime that achieves the same result for the non-Gaussian contribution. The non-Gaussian term $\lambda_0\epsilon\phi(i\tilde{g}a_0/\epsilon)$ in Eq. (35) suggests the scaling $\lambda_0 = \lambda/\epsilon, a_0 = a\,\epsilon$ considered in the main text [cf. Eq. (16)]. We now show that this is in fact the only scaling that preserves all non-Gaussian noise features, by considering general scaling exponents

$$\lambda_0 = \lambda/\epsilon^{\mu}, \qquad a_0 = a\,\epsilon^{\nu}. \tag{36}$$

Expanding then the function ϕ yields

$$\phi(i\tilde{g}/\epsilon) = \frac{a_0^2\langle x^2\rangle}{\epsilon^2}\frac{(i\tilde{g})^2}{2!} + \frac{a_0^3\langle x^3\rangle}{\epsilon^3}\frac{(i\tilde{g})^3}{3!} + \ldots \tag{37}$$

so that the $O(\tilde{g}^n)$ term of $\lambda_0\epsilon\phi$ scales as $\epsilon^{1-\mu+n(\nu-1)}$. The exponents μ, ν thus define different scaling regimes for $\epsilon \to 0$ as shown in Fig. 4.

In regime I, all orders ($n \geq 2$) in $\tilde{g}$ diverge as $\epsilon \to 0$. In regime II, there are always some higher orders that diverge as $\epsilon \to 0$, while in regime III all orders scale to zero as $\epsilon \to 0$ so that one effectively recovers the case

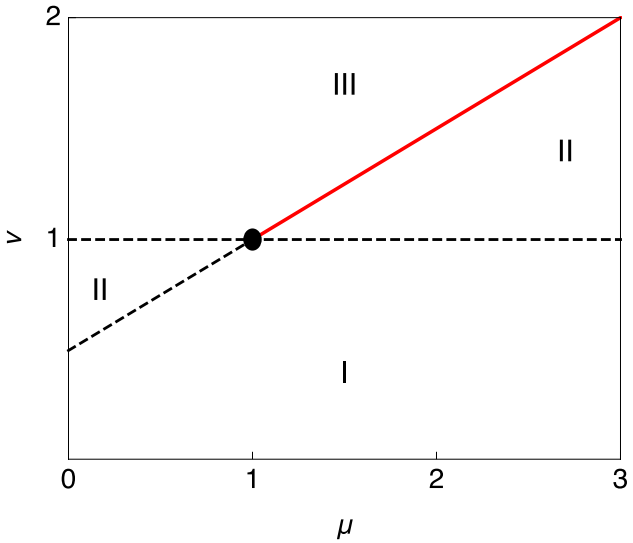

Figure 4. Different noise regimes arising under the scaling $\lambda_0 = \lambda/\epsilon^\mu, a_0 = a\,\epsilon^\nu$ in the limit $\epsilon \to 0$.

$\lambda_0 = 0$. For the particular combination $\nu = \frac{1}{2}(\mu + 1)$ with $\mu > 1$ (red line in Fig. 4) only the $\tilde{g}^2$ term remains in Eq. (37) as $\epsilon \to 0$. The non-Gaussian noise strength $\lambda_0 a_0^2 \propto \epsilon \to 0$ here, so this is a valid weak noise-limit but one that reduces to effective Gaussian noise. Only for $\mu = \nu = 1$ do all orders in $\tilde{g}$ remain in Eq. (37) as $\epsilon \to 0$. This is therefore the scaling we adopt: it represents a genuine weak-noise limit of our generic noise, since the noise variance is $D_0 + \lambda_0 a_0^2 = (D + \lambda a^2)\epsilon \propto \epsilon$ while the infinite hierarchy of noise cumulants is retained. The action then simplifies to $S[q, \tilde{g}] = \tilde{S}[q, \tilde{g}]/\epsilon$ with

$$\tilde{S}[q, \tilde{g}] = \int_0^t \mathrm{d}s \left\{ i\tilde{g}[\dot{q} + V'(q)] + \frac{\tilde{g}^2}{2} - \lambda\phi(i\tilde{g}a) \right\} \tag{38}$$

and contains ϵ only through the overall scale ϵ^{-1} as desired. The path probabilities are as before except for the scaling of the conjugate variables,

$$P[q] = \int \mathcal{D}\left[\frac{\tilde{g}}{2\pi\epsilon}\right] e^{-\tilde{S}[q,\tilde{g}]/\epsilon}. \tag{39}$$

Saddle-point integration. With the above large deviation form of the path probability, a path-integral expression for the propagator of the dynamics Eq. (2), i.e., the probability of reaching a given $q(t)$ from some $q(0)$, can be obtained by integrating over all paths with those end points. For $\epsilon \to 0$, this propagator is dominated by the path that makes the action Eq. (38) stationary, which can be found by solving the associated Euler-Lagrange equations for $q(s), \tilde{g}(s)$. However, these presume continuous paths and we find that for some non-Gaussian noise types such solutions do not exist for low λ. But we can obtain a description that extends to this more difficult regime by first eliminating $\tilde{g}$ in Eqs. (38) and (39) by saddle point integration in the weak noise limit $\epsilon \to 0$. Technically we discretize into small time intervals Δt and take $\epsilon \to 0$ first, then $\Delta t \to 0$. The stationarity condition

$$0 = i[\dot{q} + V'(q)] + \tilde{g} - i\lambda a\phi'(i\tilde{g}a) \tag{40}$$

shows that $\tilde{g}$ is imaginary at the saddle point, so in terms of $k = i\tilde{g}$ the resulting contribution to the action can be written as

$$\begin{aligned} \mathcal{L}(f) &= \max_k \{kf - k^2/2 - \lambda\phi(ak)\} \\ &= \max_k \{kf - \psi(k)\} \end{aligned} \tag{41}$$

with $f = \dot{q} + V'(q)$. The maximum rather than minimum appears here because of the saddle structure of the stationary point. One can check that this result remains valid even when ϕ has singularities on the real axis; the maximum in Eq. (41) then has to be taken over the range where ϕ remains non-singular. In our examples in Fig. 1 such singularities occur for the Gamma and exponential noise amplitude distributions. In contrast, distributions with tails decaying faster than exponentially do not exhibit such singularities; see the constant modulus example in Fig. 1.

Methods C: Analysis of the escape behaviour. *Parameter regime for non-Gaussian effects.* To understand the reduction in $S_{\min}$ as a function of λ and a we write Eq. (12) with Eq. (9) as

$$\tilde{k}^* = ak^*, \qquad V'(q) = \frac{1}{2a}\,\tilde{k}^* + \lambda a \frac{\phi_0(\tilde{k}^*)}{\tilde{k}^*}. \tag{42}$$

The terms on the right are both positive so if either of the prefactors are large ($1/a \gg 1$ or $\lambda a \gg 1$) this will force $\tilde{k}^*$ to be small. Now for small arguments $\phi(u) \approx u^2/2$ and one obtains $\tilde{k}^* = 2V'/(a^{-1} + \lambda a)$. Bearing in mind that $k^* = \tilde{k}^*/a$, the minimum action $S_{\min}$ from Eq. (11) then takes the Gaussian value, $S_{\min} \approx S_G$. Likewise, the instanton in this regime will assume the Gaussian shape, since $\psi(k) \approx (1 + \lambda a^2)k^2/2$ and Eq. (13) yields $\dot{q} = V'(q)$.

Summarizing, we predict Gaussian behaviour when $1/a \gg 1$ or $\lambda a \gg 1$. Conversely, to see non-Gaussian noise effects we need the noise amplitude to lie in the range $1 \ll a \ll 1/\lambda$; such a range exists for $\lambda \ll 1$. These predictions are consistent with the data shown in Fig. 2a,b.

Comparison with literature results for the action in special cases. We briefly review literature results where analytical predictions for the effective action $S_{\min}$ of the escape problem have been obtained for special cases of our general non-Gaussian noise as defined in Eqs. (5) and (6).

In[35,36,39], one-sided Poissonian shot noise with exponentially distributed amplitudes was considered, which corresponds to $\rho(x) = e^{-x}/2$ for $x > 0$ once we impose our normalization $\int \mathrm{d}x\, x^2 \rho(x) = 1$. With Eq. (6) we obtain the associated moment generator

$$\phi(u) = \frac{u^2}{2(1-u)} \tag{43}$$

and we also have $D = 0$ due to the absence of a Gaussian component. The condition for k^*, Eq. (12), is thus

$$V'(q) = \lambda a^2 \frac{k^*}{2(1-ak^*)} \tag{44}$$

and solving for k^* yields the action with Eq. (11)

$$S_{\min} = \int_{q_a}^{q_b} \mathrm{d}q\, \frac{2V'(q)}{\lambda a^2 + 2aV'(q)}, \tag{45}$$

which has been obtained in[35,36,39].

In[42], the authors consider one-sided Poissonian shot noise with constant one-sided amplitudes, where $\rho(x) = \delta(x-1)$ and thus

$$\phi(u) = e^u - u - 1. \tag{46}$$

In this case, Eq. (12) cannot be solved in closed form for k^*. Rearranging Eq. (12) with $D = 0$ yields k^* as the solution of

$$k^* = \frac{1}{a} \ln\left(1 + \left(a + \frac{V'(q)}{\lambda}\right)k^*\right), \tag{47}$$

and the action obtained via Eq. (11) recovers the result in[42].

In[41], the authors consider a combination of Gaussian noise and two-sided Poissonian shot noise with exponentially distributed amplitudes, which is one of the cases considered in the main text. Rearranging Eq. (12) for the type B case of Fig. 1 yields k^* as the solution of

$$k^* = \frac{2V'(q)}{D + \lambda a^2/(1 - a^2k^{*2})}. \tag{48}$$

Equation (11) with this expression for k^* matches the result obtained in[41], bearing in mind the difference by a factor 2 due to the different noise intensity conventions used.

Methods D: Escape rate calculation for a tracer particle diffusing in an active suspension. In order to obtain theoretical predictions on the escape rate for the tracer particle diffusing in an active suspension for the setup of Ref.[17], we fit the function ϕ from the tracer statistics established in[17] using the following steps:

1. We start with the data for the tracer displacement PDF $P_{\Delta t}(|\Delta X|)$ displayed in Fig. 2 of[17] for the time increment $\Delta t = 10^4$. This time interval is long enough such that the tracer statistics is in the Lévy-flight regime.
2. From the normalized displacement PDF we determine the moment generating function of the displacements for a set of k-values $\{k_1, \ldots, k_n\}$

$$\left\langle e^{k_i \Delta X} \right\rangle = \int_{-x_{\max}}^{x_{\max}} e^{k_i \Delta X} P_{\Delta t}(|\Delta X|)\mathrm{d}\Delta X, \tag{49}$$

where $x_{\max} = 2.7$ is the maximal ΔX value in the empirical PDF. The set of k-values is chosen such as to cover the range needed later in the numerical solution of Eq. (12).

3. We assume that the PDF of displacements is generated by an underlying Lévy process, which implies that $\left\langle e^{k\Delta X}\right\rangle = e^{\lambda\Delta t\,\phi(k)}$ and thus

$$\lambda\phi(k_i) = (\Delta t)^{-1} \ln\left\langle e^{k_i \Delta X}\right\rangle, \tag{50}$$

leading to a discrete representation of $\lambda\phi(k)$ obtained from the data.

4. The discrete representation is then fitted by a regression function $\hat{\phi}$ given as a superposition of ϕ-functions corresponding to constant amplitude jumps:

$$\hat{\phi}(k) = \sum_{i=1}^{m} a_i(\cosh(k\, b_i) - 1). \tag{51}$$

Here, $\{b_1, \ldots, b_m\}$ parametrize different amplitudes over a suitable range and the scale parameters $\{a_1, \ldots, a_m\}$ are determined by least squares minimization.

5. Finally, we numerically solve Eq. (12) with the fitted $\hat{\phi}(k)$ of Eq. (51) to determine the effective action for the given potential.

Data availability

The datasets used and/or analyzed during the current study are available from the corresponding author upon reasonable request.

Received: 9 November 2022; Accepted: 27 February 2023
Published online: 08 March 2023

References

1. Hänggi, P., Talkner, P. & Borkovec, M. Reaction-rate theory: fifty years after Kramers. *Rev. Mod. Phys.* **62**, 251–341 (1990).
2. Bryngelson, J. D. & Wolynes, P. G. Spin glasses and the statistical mechanics of protein folding. *PNAS* **84**, 7524–7528 (1987).
3. Auer, S. & Frenkel, D. Prediction of absolute crystal-nucleation rate in hard-sphere colloids. *Nature* **409**, 1020 (2001).
4. Whitelam, S. & Jack, R. L. The statistical mechanics of dynamic pathways to self-assembly. *Annu. Rev. Phys. Chem.* **66**, 143–163 (2015).
5. Arrhenius, S. *J. Phys. Chem.* **4**, 226 (1889).
6. Eyring, H. The activated complex in chemical reactions. *J. Chem. Phys.* **3**, 107–115 (1935).
7. Kramers, H. Brownian motion in a field of force and the diffusion model of chemical reactions. *Physica* **7**, 284–304 (1940).
8. Bovier, A. & den Hollander, F. *Metastability* (Springer, 2015).
9. MacKintosh, F. C. & Schmidt, C. F. Active cellular materials. *Curr. Opin. Cell Biol.* **22**, 29–35 (2010).
10. Toyota, T., Head, D. A., Schmidt, C. F. & Mizuno, D. Non-Gaussian athermal fluctuations in active gels. *Soft Matter* **7**, 3234 (2011).
11. Wang, B., Anthony, S. M., Bae, S. C. & Granick, S. Anomalous yet Brownian. *PNAS* **106**, 15160–15164 (2009).
12. Chen, K., Wang, B. & Granick, S. Memoryless self-reinforcing directionality in endosomal active transport within living cells. *Nat. Mater.* **14**, 589 (2015).
13. Ariga, T., Tateishi, K., Tomishige, M. & Mizuno, D. Noise-induced acceleration of single molecule kinesin-1. *Phys. Rev. Lett.* **127**, 178101 (2021).
14. Leptos, K. C., Guasto, J. S., Gollub, J. P., Pesci, A. I. & Goldstein, R. E. Dynamics of enhanced tracer diffusion in suspensions of swimming eukaryotic microorganisms. *Phys. Rev. Lett.* **103**, 198103 (2009).
15. Krishnamurthy, S., Ghosh, S., Chatterji, D., Ganapathy, R. & Sood, A. K. A micrometre-sized heat engine operating between bacterial reservoirs. *Nat. Phys.* **12**, 1134 (2016).
16. Kurihara, T., Aridome, M., Ayade, H., Zaid, A. & Mizuno, D. Non-Gaussian limit fluctuations in active swimmer suspensions. *Phys. Rev. E* **95**, 030601 (2017).
17. Kanazawa, K., Sano, T. G., Cairoli, A. & Baule, A. Loopy Lévy flights enhance tracer diffusion in active suspensions. *Nature* **579**, 364–367 (2020).
18. Sung, Y. *et al.* Non-Gaussian noise spectroscopy with a superconducting qubit sensor. *Nat. Commun.* **10**, 3715 (2019).
19. Ankerhold, J. Detecting charge noise with a Josephson junction: A problem of thermal escape in presence of non-Gaussian fluctuations. *Phys. Rev. Lett.* **98**, 036601 (2007).
20. Huard, B. *et al.* Josephson junctions as detectors for non-Gaussian noise. *Ann. Phys.* **16**, 736–750 (2007).
21. Sukhorukov, E. V. & Jordan, A. N. Stochastic dynamics of a Josephson junction threshold detector. *Phys. Rev. Lett.* **98**, 136803 (2007).
22. Grabert, H. Theory of a Josephson junction detector of non-Gaussian noise. *Phys. Rev. B* **77**, 205315 (2008).
23. Sims, D. W. *et al.* Scaling laws of marine predator search behaviour. *Nature* **451**, 1098 (2008).
24. Humphries, N. E. *et al.* Environmental context explains Lévy and Brownian movement patterns of marine predators. *Nature* **465**, 7301 (2010).
25. Ditlevsen, P. D. Observation of alpha-stable noise induced millennial climate changes from an ice-core record. *Geophys. Res. Lett.* **26**, 1441–1444 (1999).
26. Cont, R. & Tankov, P. *Financial Modelling with Jump Processes* (Chapman and Hall/CRC, 2003).
27. Schnitzer, M. J. Theory of continuum random walks and application to chemotaxis. *Phys. Rev. E* **48**, 2553–2568 (1993).
28. Tailleur, J. & Cates, M. E. Statistical mechanics of interacting run-and-tumble bacteria. *Phys. Rev. Lett.* **100**, 218103 (2008).
29. Fodor, E., Hayakawa, H., Tailleur, J. & van Wijland, E. Non-Gaussian noise without memory in active matter. *Phys. Rev. E* **98**, 062610 (2018).
30. Bouchet, F. & Reygner, J. Generalisation of the Eyring–Kramers transition rate formula to irreversible diffusion processes. *Ann. Henri Poincaré* **17**, 3499–3532 (2016).
31. Kanazawa, K., Sano, T. G., Sagawa, T. & Hayakawa, H. Minimal model of stochastic athermal systems: Origin of non-Gaussian noise. *Phys. Rev. Lett.* **114**, 090601 (2015).
32. Kanazawa, K., Sano, T. G., Sagawa, T. & Hayakawa, H. Asymptotic derivation of Langevin-like equation with non-Gaussian noise and its analytical solution. *J. Stat. Phys.* **160**, 1294–1335 (2015).

33. Baule, A. Universal Poisson statistics of a passive tracer diffusing in dilute active suspensions. (2022). http://arxiv.org/abs/2206.14078.
34. Koponen, I. Analytic approach to the problem of convergence of truncated Lévy flights towards the Gaussian stochastic process. *Phys. Rev. E* **52**, 1197 (1995).
35. Van den Broeck, C. & Hänggi, P. Activation rates for nonlinear stochastic flows driven by non-Gaussian noise. *Phys. Rev. A* **30**, 2730–2736 (1984).
36. Sancho, J. M. External dichotomous noise: The problem of the mean-first-passage time. *Phys. Rev. A* **31**, 3523–3525 (1985).
37. Masoliver, J. First-passage times for non-Markovian processes: Shot noise. *Phys. Rev. A* **35**, 3918–3928 (1987).
38. Hernández-Garcia, E., Pesquera, L., Rodriguez, M. A. & San Miguel, M. First-passage time statistics: Processes driven by Poisson noise. *Phys. Rev. A* **36**, 5774–5781 (1987).
39. Porrà, J. M. & Masoliver, J. Bistability driven by white shot noise. *Phys. Rev. E* **47**, 1633–1641 (1993).
40. Laio, F., Porporato, A., Ridolfi, L. & Rodriguez-Iturbe, I. Mean first passage times of processes driven by white shot noise. *Phys. Rev. E* **63**, 036105 (2001).
41. Gera, T. & Sebastian, K. L. Solution to the Kramers barrier crossing problem caused by two noises: Thermal noise and Poisson white noise. *J. Chem. Phys.* **155**, 014902 (2021).
42. Billings, L., Dykman, M. I. & Schwartz, I. B. Thermally activated switching in the presence of non-Gaussian noise. *Phys. Rev. E* **78**, 051122 (2008).
43. Dykman, M. I. Poisson-noise-induced escape from a metastable state. *Phys. Rev. E* **81**, 051124 (2010).
44. Khovanov, I. A. & Khovanova, N. A. Numerical simulations versus theoretical predictions for a non-Gaussian noise induced escape problem in application to full counting statistics. *Phys. Rev. B* **89**, 085419 (2014).
45. Ditlevsen, P. D. Anomalous jumping in a double-well potential. *Phys. Rev. E* **60**, 172–179 (1999).
46. Bao, J. D., Wang, H. Y., Jia, Y. & Zhuo, Y. Z. Cancellation phenomenon of barrier escape driven by a non-Gaussian noise. *Phys. Rev. E* **72**, 051105 (2005).
47. Chechkin, A. V., Gonchar, V. Y., Klafter, J. & Metzler, R. Barrier crossing of a Lévy flight. *EPL* **72**, 348 (2005).
48. Dybiec, B., Gudowska-Nowak, E. & Hänggi, P. Lévy–Brownian motion on finite intervals: Mean first passage time analysis. *Phys. Rev. E* **73**, 046104 (2006).
49. Dybiec, B., Gudowska-Nowak, E. & Hänggi, P. Escape driven by α-stable white noises. *Phys. Rev. E* **75**, 021109 (2007).
50. Chechkin, A. V., Sliusarenko, O. Y., Metzler, R. & Klafter, J. Barrier crossing driven by Lévy noise: Universality and the role of noise intensity. *Phys. Rev. E* **75**, 041101 (2007).
51. Chen, H., Duan, J., Li, X. & Zhang, C. A computational analysis for mean exit time under non-Gaussian Lévy noises. *Appl. Math. Comput.* **218**, 1845–1856 (2011).
52. Gao, T., Duan, J., Li, X. & Song, R. Mean exit time and escape probability for dynamical systems driven by Lévy noises. *SIAM J. Sci. Comput.* **36**, A887–A906 (2014).
53. Li, H., Xu, Y., Metzler, R. & Kurths, J. Transition path properties for one-dimensional systems driven by Poisson white noise. *Chaos Solitons Fract.* **141**, 110293 (2020).
54. Imkeller, P., Pavlyukevich, I. & Wetzel, T. First exit times for Lévy-driven diffusions with exponentially light jumps. *Ann. Probab.* **37**, 530–564 (2009).
55. Imkeller, P., Pavlyukevich, I. & Wetzel, T. The hierarchy of exit times of Lévy-driven Langevin equations. *Eur. Phys. J. Spec. Top.* **191**, 211–222 (2010).
56. Grafke, T., Schäfer, T. & Vanden-Eijnden, E. Sharp asymptotic estimates for expectations, probabilities, and mean first passage times in stochastic systems with small noise. (2021). http://arxiv.org/abs/2103.04837.
57. Bouchet, F. & Reygner, J. Path integral derivation and numerical computation of large deviation prefactors for non-equilibrium dynamics through matrix Riccati equations. (2021). http://arxiv.org/abs/2108.06916.
58. Caroli, B., Caroli, C. & Roulet, B. Diffusion in a bistable potential: The functional integral approach. *J. Stat. Phys.* **26**, 83 (1981).
59. Weiss, U. Decay of unstable states in macroscopic systems. *Phys. Rev. A* **25**(4), 2444–2447 (1982).
60. Bray, A. J. & McKane, A. J. Instanton calculation of the escape rate for activation over a potential barrier driven by colored noise. *Phys. Rev. Lett.* **62**, 493–496 (1989).
61. Kleinert, H. *Path Integrals in Quantum Mechanics, Statistics, Polymer Physics, and Financial Markets* (World Scientific, 2009).
62. Freidlin, M. I. & Wentzell, A. D. *Random Perturbations of Dynamical Systems* 2nd edn. (Springer, 1998).
63. Luckock, H. C. & McKane, A. J. Path integrals and non-Markov processes. III. calculation of the escape-rate prefactor in the weak-noise limit. *Phys. Rev. A* **42**, 1982–1996 (1990).
64. Sollich, P. & Baule, A. (2022). In preparation.
65. Allen, R. J., Valeriani, C. & ten Wolde, P. R. Forward flux sampling for rare event simulations. *J. Phys. Cond. Matter.* **21**, 463102 (2009).
66. Haji-Akbari, A. Forward-flux sampling with jumpy order parameters. *J. Chem. Phys.* **149**, 072303 (2018).
67. Roy, N., Leroux, N., Sood, A. K. & Ganapathy, R. Tuning the performance of a micrometer-sized Stirling engine through reservoir engineering. *Nat. Commun.* **12**, 4927 (2021).
68. Roma, D. M., O'Flanagan, R. A., Ruckenstein, A. E., Sengupta, A. M. & Mukhopadhyay, R. Optimal path to epigenetic switching. *Phys. Rev. E* **71**, 011902 (2005).
69. Woillez, E., Zhao, Y., Kafri, Y., Lecomte, V. & Tailleur, J. Activated escape of a self-propelled particle from a metastable state. *Phys. Rev. Lett.* **122**, 258001 (2019).
70. Wexler, D., Gov, N., Rasmussen, K. Ø. & Bel, G. Dynamics and escape of active particles in a harmonic trap. *Phys. Rev. Res.* **2**, 013003 (2020).
71. Martin, P. C., Siggia, E. D. & Rose, H. A. Statistical dynamics of classical systems. *Phys. Rev. A* **8**, 423–437 (1973).
72. Hertz, J. A., Roudi, Y. & Sollich, P. Path integral methods for the dynamics of stochastic and disordered systems. *J. Phys. A* **50**, 033001 (2016).

Acknowledgements

We gratefully acknowledge helpful discussions with Rob Jack and Kiyoshi Kanazawa. We thank Tomohiko Sano for sharing the simulation data and code of Ref.[17].

Author contributions

A.B. and P.S. designed the research, performed analytical and numerical computations, analysed the data, and wrote the paper.

Competing interests

The authors declare no competing interests.

Additional information

Correspondence and requests for materials should be addressed to A.B.

Reprints and permissions information is available at www.nature.com/reprints.

Publisher's note Springer Nature remains neutral with regard to jurisdictional claims in published maps and institutional affiliations.